Mixed bubbles in a one-dimensional Bose-Bose mixture

P. Stürmer,* M. Nilsson Tengstrand, and S. M. Reimann

Mathematical Physics and NanoLund, Lund University, Box 118, 22100 Lund, Sweden

(Received 26 July 2022; accepted 7 November 2022; published 12 December 2022)

We investigate a Bose-Bose mixture across the miscible-immiscible phase transition governed by quantum fluctuations in one dimension. We find the recently predicted so-called mixed bubbles as ground states close to the mean-field miscible-immiscible threshold. These bubbles form a pocket of miscibility, separated by one of the components. The collective excitations reflect the symmetry breaking resulting from the bubble formation. The partial miscibility of the system allows for persistent currents in an annular confinement. Intriguingly, the mixed bubble acts like an intrinsic weak link, connecting the rotational behavior of the mixed bubble state to current efforts in atomtronic applications.

DOI: 10.1103/PhysRevResearch.4.043182

I. INTRODUCTION

In the mean-field (MF) approximation the phase of a two-component Bose-Bose mixture is dominated by its interaction coupling strengths $g_{\sigma\sigma'}$ between the components 1 and 2 with particle densities n_1 and n_2. The system is determined by $\delta g = g_{12} - \sqrt{g_{11}g_{22}}$ and may be in a miscible phase if $\delta g < 0$ and in an immiscible phase if $\delta g > 0$ [1,2]. Experiments on Bose-Bose mixtures have shown the phase transition of repulsive mixtures from miscible to immiscible [3,4], in agreement with theoretical predictions [5,6]. This interplay of interactions can also lead to such exotic states as dark/bright solitons [7–9], magnetic solitons [10–12], or even dark/dark/bright and dark/bright/bright solitons in three-component mixtures [13] and the number of members in this family of states is ever increasing. The inclusion of corrections beyond the mean field has added a novel class of phases, where quantum fluctuations [14,15] may stabilize the system against collapse, as predicted for a two-component Bose-Bose mixture [16] and first observed in a mixture of a one-component dipolar gas [17,18]. The original proposal for a self-bound state in a binary mixture was subsequently also realized experimentally [19,20]. The observed liquefaction into self-bound droplets has led to vivid research into their dimensional properties [21], dynamics [22], and behavior under rotation [23–25]. Additionally, the anisotropic dipolar interaction was found to allow for realization of the long-sought state of supersolidity [26–29], exhibiting a phase and amplitude mode due to its spontaneous symmetry breaking [30]. Current efforts focus on, e.g., nonzero-temperature behavior [31], rotational properties [32,33], and dipolar-contact [34] and dipolar-dipolar [35] mixtures. While the aforementioned works focused on the effect of quantum fluctuations on the stabilization against collapse, Ref. [36] suggests that for repulsive two-component Bose-Bose mixtures quantum fluctuations likewise may lead to a new phase of matter in between the miscible-immiscible phase transition, a so-called mixed bubble phase. The proposal of this new phase is based on a transformation of the densities $n_{1,2}$ to $n_\pm$ [16,36] as

$$n_\pm = \frac{\alpha^{-1/2} n_1 \pm \alpha^{1/2} n_2}{\sqrt{\alpha + \alpha^{-1}}}, \tag{1}$$

where $\alpha = \sqrt{g_{22}/g_{11}}$. Along n_+ the system's behavior is dominated by the MF contribution, while along n_- the system is sensitive to the usually much weaker quantum fluctuations. This separation of scales allows the grand potential density to predict the onset of new phases along n_-, for which it is a convex function if the system is miscible and a concave function if the system is immiscible. However, close to the phase transition, where quantum fluctuations become comparable in size to the MF contribution, the grand potential density may be a concave-convex function for $\alpha < 1$ or a convex-concave function for $\alpha > 1$, allowing for a new phase to emerge. As mentioned above, this new phase has been dubbed a mixed bubble in a Bose-Bose mixture [36] and can be seen as a pocket of one component trapped within the gaseous medium of the other component. Little is known about its properties. In this work we investigate the formation of these novel mixed bubbles in a one-dimensional annular confinement close to the miscible-immiscible threshold. The annular confinement leaves the subtle balance between quantum fluctuations and the mean field undisturbed, a requirement for the formation of mixed bubbles [36]. We start by exploring the shape of mixed bubbles for a set of population imbalances between the components, probing the predictions made in Ref. [36] for a uniform infinite system by varying the criticality parameter $\sqrt{n_+}\delta g/g^{3/2}$. We show that for a binary mixture in a ring, a localized pocket of one component coexists with a nonvanishing part of the second component, resulting in a

*philipp.sturmer@matfys.lth.se

pocket of miscibility within an immiscible mixture. The annular confinement introduces finite-size effects that persist in the thermodynamic limit, which can be obtained as a correcting factor depending on the interaction and particle-number imbalances of the originally proposed critical value. Classifying the miscible-bubble-immiscible phase transition via its collective excitations, a phase (Goldstone) and an amplitude (Higgs) mode can be identified. Further, the mixed bubble can support persistent currents in an annular confinement, however exhibiting an avoided level crossing of rotational states due to a repulsive intercomponent interaction, leading to the analogy of an intrinsic weak link [37–39]. From here on, we follow the notation in Ref. [36] and signify the miscible phase as $1+2$, the immiscible phase as $1|2$, and the mixed bubble as $(1+2)|2$ if $\alpha < 1$ and $(1+2)|1$ if $\alpha > 1$. Note that, according to Ref. [36], this phase cannot occur for $\alpha = 1$.

II. MODEL

A uniform Bose-Bose mixture in one dimension with equal masses of atoms but potentially unequal short-range interactions, including beyond-mean-field effects in the Bogoliubov approximation, has energy

$$E = \sum_{\sigma} E_{\mathrm{kin},\sigma} + \sum_{\sigma,\sigma'} \frac{g_{\sigma\sigma'}}{2} n_\sigma n_{\sigma'} + E_{\mathrm{B}}, \tag{2}$$

where E_{B} is the Bogoliubov vacuum energy. In one dimension and for homonuclear components, E_{B} can be written as

$$-\frac{2}{3\pi}\frac{m^2}{\hbar}\sum_{\pm} c_{\pm}^3, \tag{3}$$

where the squared Bogoliubov sound velocities are [21]

$$c_{\pm}^2 = \frac{g_{11}n_1 + g_{22}n_2 \pm \sqrt{(g_{11}n_1 - g_{22}n_2)^2 + 4g_{12}^2 n_1 n_2}}{2m}. \tag{4}$$

The Bogoliubov vacuum energy in Eq. (3) is only valid provided the weak-interaction parameter $\eta_{1\mathrm{D}} \approx \sqrt{mg/n}/\hbar \ll 1$. Further, assuming $\delta g \approx \eta_{1\mathrm{D}}$, we set $\delta g = 0$ in the sound velocities $c_{\pm}$ in Eq. (4). The chemical potentials μ_σ of the components are then given by $\mu_\sigma = \partial E/\partial n_\sigma$ and give rise to the respective stationary extended Gross-Pitaevskii equations

$$\mu_\sigma \psi_\sigma = \left[-\frac{\hbar^2}{2m}\partial_{\theta\theta} + g_{\sigma\sigma} n_\sigma + g_{\sigma\sigma'} n_{\sigma'} - \frac{m^{1/2} g_{\sigma\sigma}}{\pi\hbar}\left(\sum_{\sigma} g_{\sigma\sigma} n_\sigma\right)^{1/2} \right]\psi_\sigma. \tag{5}$$

We impose periodic boundary conditions $\psi_\sigma(\theta) = \psi_\sigma(\theta + 2\pi R)$, thus enforcing an annular confinement of circumference $2\pi R$. We set $g = \sqrt{g_{11}g_{22}}$ and use dimensionless units $m = \hbar = R = 1$. The order parameter is normalized to the number of particles N_σ in each component according to $\int_{-\pi}^{\pi} d\theta |\psi_\sigma(\theta)|^2 = N_\sigma$. The ground state of Eq. (5) is obtained by imaginary-time propagation using a split-step Fourier method. Later in this paper we analyze the system under rotation, which requires adding a $-\Omega\hat{L}\psi_\sigma$ on the right-hand side of Eq. (5), with $\hat{L} = -i\partial_\theta$. We also enforce a fixed value of angular momentum $L = L_1 + L_2$, where $L_\sigma = \int_{-\pi}^{\pi} d\theta\, \psi_\sigma^* \hat{L}\psi_\sigma$ as described in [23,40]. Introducing $N = N_1 + N_2$ and $\nu = N_1/N_2$, we illustrate our findings for a repulsive homonuclear two-component system and $\alpha = 2.7$, $g = 5.0$, and $N = 10\,000$. The chosen parameters are proposed to be experimentally reachable configurations to observe the mixed bubble phase in three dimensions for a system of ^{41}K-^{39}K, both in hyperfine states $F = 1$, $m_{\mathrm{F}} = 0$ [36,41,42]. In order to sample the phase transition, we vary g_{12} by changing $\sqrt{n_+}\delta g/g^{3/2}$, using the uniform values for n_σ in Eq. (1).

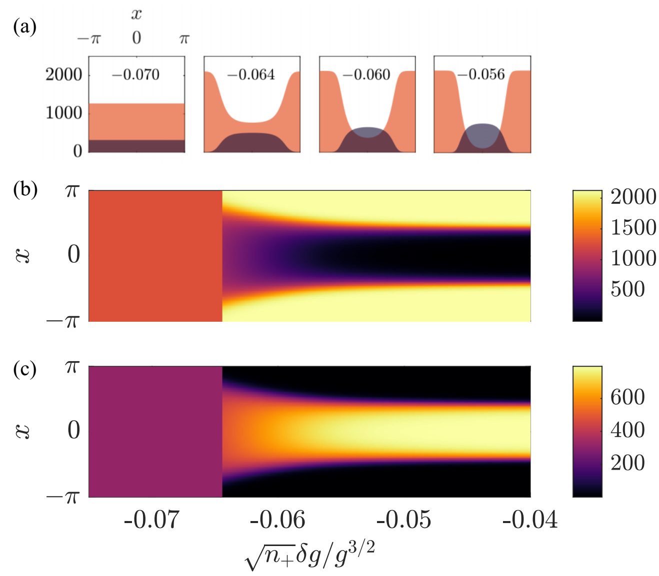

FIG. 1. (a) Density distributions for four different parameters of $\sqrt{n_+}\delta g/g^{3/2}$ as indicated in the figures, with the orange and black components corresponding to the first and second components, respectively. The first distribution shows the system in a miscible state, while the remaining distributions show the system in a mixed bubble state. Also shown are the density distributions in the ring for $\nu = 4.0$ along the criticality parameter $\sqrt{n_+}\delta g/g^{3/2}$ for (b) the first and (c) the second component. By increasing $\sqrt{n_+}\delta g/g^{3/2}$ the components start to localize on opposite sides of the ring, resulting in the coexistence of a mixed and separated phase until it reaches full phase separation.

III. DENSITY DISTRIBUTIONS

We first investigate the existence of the mixed bubble phase and the corresponding density distributions for the above choice of parameters. The predicted range in Eqs. (16) and (17) of Ref. [36] for an infinite uniform system lies within

$$\frac{\delta g_{\min}}{g^{3/2}}\sqrt{n_+} = -\frac{1}{4\pi}\frac{(\alpha-1)^2}{\sqrt{\alpha}(\alpha^2+1)^{1/4}},$$
$$\delta g_{\max} = \frac{4(\sqrt{\alpha}+2)}{3(\sqrt{\alpha}+1)^2}\delta g_{\min}. \tag{6}$$

Inserting $\alpha = 2.7$ then gives the range of $[-0.082, -0.057]$. We continue by choosing $\nu = 4.0$. Figure 1(a) shows examples of density distributions for four values of the criticality parameter, with the first component $|\psi_1|^2$ in orange and the second component $|\psi_2|^2$ in black. Figures 1(b) and 1(c) show the full phase transition across the criticality parameter $\sqrt{n_+}\delta g/g^{3/2}$ as surface plots of both components. As g_{12}

increases, the components begin to localize on opposite sides of the ring, shifted by π. This leads to the predicted coexistence of immiscibility and miscibility induced by quantum fluctuations. As one continues to move towards immiscibility, the mixed part of the first component decreases linearly in density with increasing g_{12}, while the second component's pocket increases in density, reducing its width, eventually resulting in immiscibility by further increasing g_{12}. Without the Bogoliubov vacuum energy E_B in Eq. (2) the system would still be in a fully miscible regime. Note that the observed values at which the phase transition occurs differ significantly from the one predicted in Eq. (6). Further, the exact range of $(\delta g_{\min}, \delta g_{\max})$ depends strongly on the exact value of the particle ratio ν. This may be due to finite-size effects, compared to the prediction in Ref. [36], which assumes an infinite system. (We will return to this question later, when we consider the system's collective excitations.) We also observe that the bubble phase vanishes completely as $\nu \to 1$; however, this process can be reversed for $1/\nu$ if $\alpha \to 1/\alpha$, which results in $(1+2)|2 \to (1+2)|1$. Similarly to dark/bright or magnetic solitons, the mixed bubble consists of one component localizing and the second component filling the resulting density vacancy. In the case of the dark/bright soliton this effect occurs due to imprinting a phase difference onto one component, resulting in a dark soliton [7–9,43]. For the magnetic soliton the phase difference is imprinted onto both components [10–12], leading to a similar density distribution. The stark difference from the bubble, however, lies in the fact that the solitonic systems represent excited states, while the bubble represents a ground state to bridge the phase transition from $1+2$ to $1|2$. The soliton solutions require $g - g_{12} > 0$ in a description without the Bogoliubov vacuum energy E_B in Eq. (2) [7].

IV. COLLECTIVE EXCITATIONS

Let us now discuss the collective excitations across the criticality parameter. Applying the standard procedure, we linearize the time-dependent variants of Eq. (5) to first order around the ground state $\psi_{0,\sigma}$, introducing quasiparticle amplitudes u_σ and v_σ as

$$\psi_\sigma(\theta, t) = e^{-i\mu_\sigma t}[\psi_{0,\sigma}(\theta) + u_\sigma(\theta)e^{-i\omega t} + v_\sigma^*(\theta)e^{i\omega^* t}], \quad (7)$$

with $\int_{-\pi}^{\pi} d\theta[|u_\sigma(\theta)|^2 - |v_\sigma(\theta)|^2] = 1$. The resulting Bogoliubov–de Gennes equations can for this system be written as a $4N \times 4N$ linear response eigenvalue problem $\mathbf{M}\mathbf{v} = \omega\mathbf{v}$, where N is the dimension of each block matrix, $\mathbf{v} = (u_1(x), v_1(x), u_2(x), v_2(x))^\top$, and

$$\mathbf{M} = \begin{bmatrix} X_{12} & Y_1 & Z & Z \\ -Y_1 & -X_{12} & -Z & -Z \\ Z & Z & X_{21} & Y_2 \\ -Z & -Z & -Y_2 & -X_{12} \end{bmatrix}, \quad (8)$$

with

$$X_{\sigma\sigma'} = -\frac{1}{2}\partial_{xx} + 2g_{\sigma\sigma}n_\sigma + g_{\sigma\sigma'}n_{\sigma'} - \frac{g_{\sigma\sigma}}{2\pi}\frac{3g_{\sigma\sigma}n_\sigma + 2g_{\sigma'\sigma'}n_{\sigma'}}{(g_{11}n_1 + g_{22}n_2)^{1/2}} - \mu_\sigma,$$

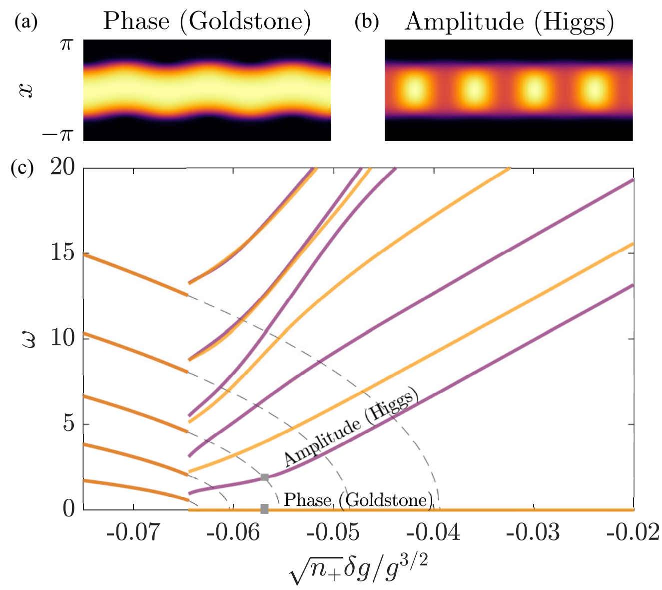

FIG. 2. Time evolution of the second component of (a) phase (Goldstone) and (b) amplitude (Higgs) modes at $\sqrt{n_+}\delta g/g^{3/2} = -0.0577$. (c) Collective excitation spectrum of the ten lowest modes for $\nu = 4.0$ across the miscible-bubble-immiscible phase transition from $\sqrt{n_+}\delta g/g^{3/2} = -0.075$ to -0.02. Modes of even parity are displayed in orange and those of odd parity in purple. The transition from miscible to bubble occurs at around -0.0651. The gray box indicates the position of the Goldstone and amplitude modes shown above. Dashed gray lines indicate the real branch of the excitation spectrum of a uniform Bose-Bose mixture as given by Eq. (12).

$$Y_\sigma = g_{\sigma\sigma}n_\sigma - \frac{g_{\sigma\sigma}}{2\pi}\frac{g_{\sigma\sigma}n_\sigma}{(g_{11}n_1 + g_{22}n_2)^{1/2}},$$

$$Z = g_{12}\sqrt{n_1n_2} - \frac{g}{2\pi}\frac{g\sqrt{n_1n_2}}{(g_{11}n_1 + g_{22}n_2)^{1/2}}. \quad (9)$$

We solve the corresponding eigenvalue problem numerically in a real Fourier collocation scheme with a locally optimal block preconditioned four-dimensional conjugate gradient method [44,45]. The obtained spectrum is displayed in Fig. 2, with even and uneven modes in orange and purple, respectively. Starting from the miscible phase, degenerate pairs of uneven and even modes split up upon transitioning from the miscible to the bubble regime. The phase transition is numerically noncontinuous in the excitation spectrum due to the external confinement up to a relative step size approximately equal to 10^{-6}, leading to a jump in excitation frequency. As the bubble localizes, spontaneous breaking of U(1) symmetry occurs, leading to a phase (Goldstone) mode in the bubble and immiscible phase. The time evolution of the phase (Goldstone) mode $|\psi_\sigma(\theta, t)|^2$ is shown in Fig. 2(a), following

$$|\psi_\sigma(\theta, t)|^2 = |\psi_{\sigma,0}(\theta)|^2 + 2f_\sigma(\theta)\psi_{\sigma,0}(\theta)\cos(\omega t), \quad (10)$$

with $f_\sigma(\theta) = u_\sigma(\theta) + v_\sigma(\theta)$ [30]. The phase (Goldstone) mode persists through the transition into the immiscible regime. We also identify an amplitude (Higgs) mode in the bubble phase. Note that the densities of both components oscillate in phase at the beginning of the amplitude mode. As g_{12} increases, the amplitude of density oscillation in the first component decreases, until it eventually oscillates out of phase with the second component. Furthermore, we calculate the lowest-lying excitations in the uniform regime by expanding $\mathbf{v}$ in plane waves due to the annular confinement as [1]

$$\mathbf{v}(x) = \sum_{p=-\infty}^{\infty} \frac{e^{ipx}}{\sqrt{2\pi}} \tilde{\mathbf{v}}_p. \tag{11}$$

Substituting this into the above linear response eigenvalue problem yields

$$\omega_{p,\pm}^2 = \frac{p^2}{4\pi}\Bigg\{p^2\pi + \sum_{\sigma,\sigma'} g_{\sigma\sigma}N_\sigma(1-g_{\sigma\sigma}\eta) \pm\Bigg[\Bigg(\sum_{\sigma,\sigma'}(-1)^{1-\sigma}g_{\sigma\sigma}N_\sigma(1-g_{\sigma\sigma}\eta)\Bigg)^2 + 4N_1N_2(g_{12}-g_{11}g_{22}\eta)^2\Bigg]^{1/2}\Bigg\}, \tag{12}$$

with $\eta = [2\pi(g_{11}N_1 + g_{22}N_2)^{1/2}]^{-1}$ and the real branches of $\omega_\pm$ shown as light gray dashed lines in Fig. 2. If one of the branches becomes imaginary, the associated phase becomes unstable. Hence one may use $\omega_{1,\pm}^2 = 0$ to estimate the critical point for the phase transition away from the miscible regime. Furthermore, taking the thermodynamic limit $N \to \infty$, we find the critical value for $p = 1$ as

$$\lim_{N\to\infty} \sqrt{n_+}\frac{\delta g}{g^{3/2}} = -\frac{1}{4\pi}\frac{(\alpha-1)^2}{\sqrt{\alpha}(\alpha^2+1)^{1/4}}\sqrt{\frac{\alpha+\nu}{\alpha^2+\nu}}. \tag{13}$$

Intriguingly, this expression is equivalent to the first of Eqs. (6) with an additional factor of $\sqrt{(\alpha+\nu)/(\alpha^2+\nu)}$, which signifies the miscible-bubble phase transition, such that the observed shift of the phase transition away from Eqs. (6) can be explained by finite-size effects emerging in the annular confinement.

V. NONRIGID ROTATIONAL-INERTIA FRACTION

The localization during the phase transition into the mixed bubble suggests that one investigate the phase transition by means of the nonrigid rotational-inertia (NRRI) fraction [46]

$$f_\sigma = 1 - \lim_{\Omega\to 0}\frac{L_\sigma}{N_\sigma\Omega}. \tag{14}$$

This quantifies the rotational behavior for small rotations by comparing the angular momentum a system picks up under rotation to the angular momentum it would have if it were rigid. As such, a uniform system will have nonrigid rotational inertia equal to unity and a rigid body equal to zero. The NRRI fraction is calculated numerically as a function of $\sqrt{n_+}\delta g/g^{3/2}$ and shown in Fig. 3 for three different values of ν. All three systems exhibit a qualitatively similar behavior, for which the NRRI fraction starts at unity for the mixed phase until criticality. As discussed before, the exact critical value depends on ν, with higher ν having a lower critical value and coinciding with the onset of localization in the density distributions. For all systems the second component's NRRI fraction (dashed line) approaches zero quickly, signifying the onset of a mixed bubble, only while the first component's NRRI fraction (solid line) slowly decreases to zero, signifying the onset of phase separation. The total NRRI fraction of a system is given by the thin lines as $f_s = (f_{s,1}\nu + f_{s,2})/(1+\nu)$.

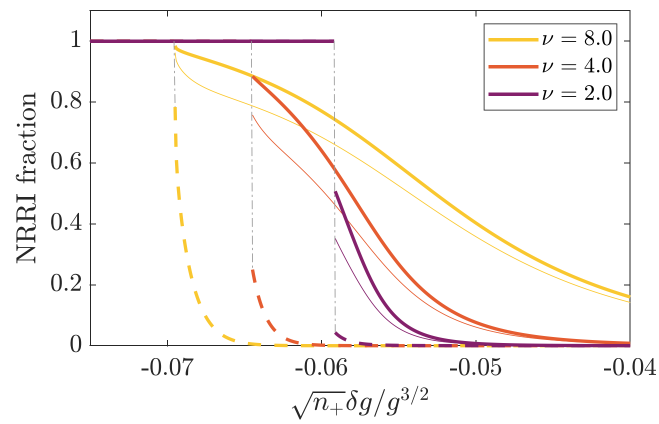

FIG. 3. Nonrigid rotational inertia for systems of varying ν across the miscible-bubble-immiscible phase transition. The second component (dashed line) follows a sharp decline upon localization, turning into a rigid body, while the first component's NRRI fraction (solid line) decreases more slowly during the bubble phase. The system's total NRRI fraction as given in the text is shown as a thin solid line.

VI. ROTATIONAL PROPERTIES

In the following we will now enforce a certain angular momentum per particle l into systems of variable $\sqrt{n_+}\delta g/g^{3/2}$ and measure its ground-state energy per particle in the nonrotating frame as $[E(l) - E(0)]/N$. In the case of a rigid body this leads to a parabola of shape $l^2/2$, while for a uniform system one obtains a concave periodic structure on top of the parabola with minima when a vortex fully nucleated at the center [47]. We plot this quantity in Fig. 4 for the given values of $\sqrt{n_+}\delta g/g^{3/2}$ and find that it follows the trajectory of dampened intersecting parabolas. Evaluating $E(l)$ dependent on a sytem's NRRI fraction [48], we show the resulting intersecting parabolas as gray dashed lines in Fig. 4 for $\nu = 4.0$, $\sqrt{n_+}\delta g/g^{3/2} = -0.064$, and a NRRI fraction of 0.7172. Here the dampening effect occurs due to an increased difficulty of the current in component 1 traversing through the mixed region, leading to a mixing of rotational states [49]. Despite the dampening effect, the system is still able to support persistent currents for some parameters. A similar dampening effect is known to occur in atomtronic applications in one-component systems of repulsive bosons where the rotational symmetry is broken by the addition of a so-called weak link to stir the condensate [50]. The mixed bubble can here be regarded as an intrinsic weak link with an avoided level crossing between the rotational states signified by the dampening effect. We calculate the spatially averaged current relative to the rotating ring $I(\Omega) = (2\pi)^{-1}\int_{-\pi}^{\pi} d\theta\, j(\theta)$, where $j(\theta) = n(\theta)v(\theta)$ is the current density. The velocity $v(\theta)$ in the rotating frame is obtained by inserting $\psi_\sigma(\theta) = \phi_\sigma(\theta)e^{i\alpha(\theta)}$ into Eq. (5) and separating the real and imaginary parts. The resulting expression for the gradient of the phase $\alpha'(\theta)$ equals the velocity $v(\theta) = (L - N\Omega)/2\pi n(\theta)$ [48]. The space-averaged current

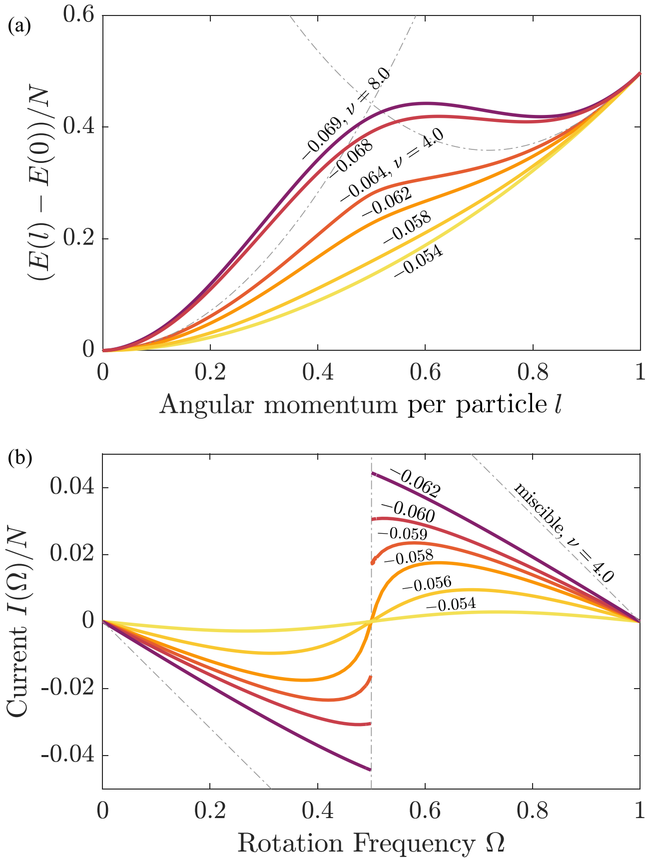

FIG. 4. (a) Rotational energy per particle in the nonrotating frame at a fixed number of angular momentum per particle l. Values of $\sqrt{n_+}\delta g/g^{3/2}$ are given in the plot. Closer to immiscibility, the energy approaches the rigid-body limit, while close to miscibility the bubble may support persistent currents for nonzero l. (b) Current $I(\Omega)/N$ through the weak link formed by the bubble. Values of $\sqrt{n_+}\delta g/g^{3/2}$ are given in the plot. Starting with a discontinuity, the current starts bending due to the constriction the bubble provides until the two branches connect at $I(0.5)/N = 0$, from which point the current moves from a smeared sawtooth function to a sinusoidal modulation with increasing intercomponent interaction.

through the weak link in the rotating frame can then be calculated as

$$I(\Omega) = \frac{1}{2\pi}\int_{-\pi}^{\pi} d\theta\, j(\theta) = \frac{L - N\Omega}{2\pi}. \tag{15}$$

The current $I(\Omega)$ is shown in Fig. 4 and our description is equivalent to the relation derived in Ref. [51] and used in Ref. [50]. Close to the miscible regime, the usual sawtooth behavior of the current obtains a small curvature, but retains its symmetric discontinuity at $\Omega \to 0.5$. The mixed bubble grows in size with increasing intercomponent interaction strength and provides a stronger obstacle to overcome for the flow in component one. Thus, the currents' branches start bending towards zero as $\Omega \to 0.5$ until they eventually connect and become continuous with $I(0.5) = 0$. The current then resembles the behavior of a one-component system with a strong weak link [50]. Initially this is displayed by a dampened sawtooth function, which moves towards a sinusoidal oscillation as the system approaches immiscibility.

VII. CONCLUSION AND OUTLOOK

Similarly to self-bound droplets, quantum fluctuations originating from the Bogoliubov vacuum energy in Eq. (3) introduce a new phase of Bose-Bose mixtures in between the miscible-immiscible phase transition confirming the recent prediction made in Ref. [36]. We found that intriguingly the mixed bubbles act like a single component trapped in a gaseous medium as a pocket of miscibility exhibiting nontrivial nonrigid rotational inertia. The annular confinement used here leads to finite-size effects, which introduce a correcting factor for the critical value in the miscible-bubble phase transition to the prediction made in Ref. [36]. When enforcing a certain amount of angular momentum on the system, the mixed bubble mimics a weak link, with an avoided level crossing between the consecutive rotational states due to the repulsive interspecies interactions. However, the system is still able to support persistent currents around the ring for some parameters, as the reduction of the cusp leads to a plateau. Our work, here restricted to an investigation of the newly discovered mixed bubble phase, opens many new questions. It would be interesting to explore bubble dynamics and to extend the analysis also to the two- and three-dimensional cases, in a nonannular trap and for a heavily-mass-imbalanced system such as a ^{174}Yb-^{7}Li mixture. Further, it may be interesting if the mixed bubble can also be found in a one-dimensional strongly interacting few-body system. Particularly interesting perspectives emerge for atomtronics applications (see the recent review [52]), where the weak link dynamics plays a crucial role.

ACKNOWLEDGMENTS

We thank J. Bengtsson and J. Bjerlin for fruitful discussions about the excitation spectrum and A. Recati for his suggestions on the solitonic structure. This work was financially supported by the Knut and Alice Wallenberg Foundation, the Swedish Research Council, and NanoLund.

[1] C. J. Pethick and H. Smith, *Bose-Einstein Condensation in Dilute Gases*, 2nd ed. (Cambridge University Press, Cambridge, 2008).
[2] L. Pitaevskii and S. Stringari, *Bose-Einstein Condensation and Superfluidity* (Oxford University Press, Oxford, 2016), Vol. 164.
[3] S. B. Papp, J. M. Pino, and C. E. Wieman, Tunable Miscibility in a Dual-Species Bose-Einstein Condensate, Phys. Rev. Lett. **101**, 040402 (2008).
[4] J. Stenger, S. Inouye, D. M. Stamper-Kurn, H.-J. Miesner, A. P. Chikkatur, and W. Ketterle, Spin domains in ground-state Bose–Einstein condensates, Nature (London) **396**, 345 (1998).

[5] B. D. Esry, C. H. Greene, J. P. Burke, Jr., and J. L. Bohn, Hartree-Fock Theory for Double Condensates, Phys. Rev. Lett. **78**, 3594 (1997).

[6] E. Timmermans, Phase Separation of Bose-Einstein Condensates, Phys. Rev. Lett. **81**, 5718 (1998).

[7] C. Becker, S. Stellmer, P. Soltan-Panahi, S. Dörscher, M. Baumert, E.-M. Richter, J. Kronjaeger, K. Bongs, and K. Sengstock, Oscillations and interactions of dark and dark-bright solitons in Bose-Einstein condensates, Nat. Phys. **4**, 496 (2008).

[8] S. Mossman, G. C. Katsimiga, S. I. Mistakidis, A. Romero-Ros, T. M. Bersano, P. Schmelcher, P. G. Kevrekidis, and P. Engels, Dense dark-bright soliton arrays in a two-component Bose-Einstein condensate, arXiv:2208.10585.

[9] M. O. D. Alotaibi and L. D. Carr, Dynamics of dark-bright vector solitons in Bose-Einstein condensates, Phys. Rev. A **96**, 013601 (2017).

[10] C. Qu, L. P. Pitaevskii, and S. Stringari, Magnetic Solitons in a Binary Bose-Einstein Condensate, Phys. Rev. Lett. **116**, 160402 (2016).

[11] X. Chai, L. You, and C. Raman, Magnetic solitons in an immiscible two-component Bose-Einstein condensate, Phys. Rev. A **105**, 013313 (2022).

[12] A. Farolfi, D. Trypogeorgos, C. Mordini, G. Lamporesi, and G. Ferrari, Observation of Magnetic Solitons in Two-Component Bose-Einstein Condensates, Phys. Rev. Lett. **125**, 030401 (2020).

[13] T. M. Bersano, V. Gokhroo, M. A. Khamehchi, J. D'Ambroise, D. J. Frantzeskakis, P. Engels, and P. G. Kevrekidis, Three-Component Soliton States in Spinor $f = 1$ Bose-Einstein Condensates, Phys. Rev. Lett. **120**, 063202 (2018).

[14] T. D. Lee, K. Huang, and C. N. Yang, Eigenvalues and eigenfunctions of a Bose system of hard spheres and its low-temperature properties, Phys. Rev. **106**, 1135 (1957).

[15] D. M. Larsen, Binary mixtures of dilute Bose gases with repulsive interactions at low temperature, Ann. Phys. (NY) **24**, 89 (1963).

[16] D. S. Petrov, Quantum Mechanical Stabilization of a Collapsing Bose-Bose Mixture, Phys. Rev. Lett. **115**, 155302 (2015).

[17] H. Kadau, M. Schmitt, M. Wenzel, C. Wink, T. Maier, I. Ferrier-Barbut, and T. Pfau, Observing the Rosensweig instability of a quantum ferrofluid, Nature (London) **530**, 194 (2016).

[18] M. Schmitt, M. Wenzel, F. Böttcher, I. Ferrier-Barbut, and T. Pfau, Self-bound droplets of a dilute magnetic quantum liquid, Nature (London) **539**, 259 (2016).

[19] G. Semeghini, G. Ferioli, L. Masi, C. Mazzinghi, L. Wolswijk, F. Minardi, M. Modugno, G. Modugno, M. Inguscio, and M. Fattori, Self-Bound Quantum Droplets of Atomic Mixtures in Free Space, Phys. Rev. Lett. **120**, 235301 (2018).

[20] C. R. Cabrera, L. Tanzi, J. Sanz, B. Naylor, P. Thomas, P. Cheiney, and L. Tarruell, Quantum liquid droplets in a mixture of Bose-Einstein condensates, Science **359**, 301 (2018).

[21] D. S. Petrov and G. E. Astrakharchik, Ultradilute Low-Dimensional Liquids, Phys. Rev. Lett. **117**, 100401 (2016).

[22] G. E. Astrakharchik and B. A. Malomed, Dynamics of one-dimensional quantum droplets, Phys. Rev. A **98**, 013631 (2018).

[23] M. N. Tengstrand, P. Stürmer, E. Ö. Karabulut, and S. M. Reimann, Rotating Binary Bose-Einstein Condensates and Vortex Clusters in Quantum Droplets, Phys. Rev. Lett. **123**, 160405 (2019).

[24] P. Stürmer, M. N. Tengstrand, R. Sachdeva, and S. M. Reimann, Breathing mode in two-dimensional binary self-bound Bose-gas droplets, Phys. Rev. A **103**, 053302 (2021).

[25] M. Caldara and F. Ancilotto, Vortices in quantum droplets of heteronuclear Bose mixtures, Phys. Rev. A **105**, 063328 (2022).

[26] L. Chomaz, D. Petter, P. Ilzhöfer, G. Natale, A. Trautmann, C. Politi, G. Durastante, R. M. W. van Bijnen, A. Patscheider, M. Sohmen, M. J. Mark, and F. Ferlaino, Long-Lived and Transient Supersolid Behaviors in Dipolar Quantum Gases, Phys. Rev. X **9**, 021012 (2019).

[27] F. Böttcher, J.-N. Schmidt, M. Wenzel, J. Hertkorn, M. Guo, T. Langen, and T. Pfau, Transient Supersolid Properties in an Array of Dipolar Quantum Droplets, Phys. Rev. X **9**, 011051 (2019).

[28] L. Tanzi, E. Lucioni, F. Famà, J. Catani, A. Fioretti, C. Gabbanini, R. N. Bisset, L. Santos, and G. Modugno, Observation of a Dipolar Quantum Gas with Metastable Supersolid Properties, Phys. Rev. Lett. **122**, 130405 (2019).

[29] L. Tanzi, S. M. Roccuzzo, E. Lucioni, F. Famà, A. Fioretti, C. Gabbanini, G. Modugno, A. Recati, and S. Stringari, Supersolid symmetry breaking from compressional oscillations in a dipolar quantum gas, Nature (London) **574**, 382 (2019).

[30] J. Hertkorn, F. Böttcher, M. Guo, J. N. Schmidt, T. Langen, H. P. Büchler, and T. Pfau, Fate of the Amplitude Mode in a Trapped Dipolar Supersolid, Phys. Rev. Lett. **123**, 193002 (2019).

[31] J. Sánchez-Baena, C. Politi, F. Maucher, F. Ferlaino, and T. Pohl, Heating a quantum dipolar fluid into a solid, arXiv:2209.00335.

[32] S. M. Roccuzzo, A. Gallemí, A. Recati, and S. Stringari, Rotating a Supersolid Dipolar Gas, Phys. Rev. Lett. **124**, 045702 (2020).

[33] M. N. Tengstrand, D. Boholm, R. Sachdeva, J. Bengtsson, and S. M. Reimann, Persistent currents in toroidal dipolar supersolids, Phys. Rev. A **103**, 013313 (2021).

[34] S. Li, U. N. Le, and H. Saito, Long-lifetime supersolid in a two-component dipolar Bose-Einstein condensate, Phys. Rev. A **105**, L061302 (2022).

[35] T. Bland, E. Poli, L. A. P. Ardila, L. Santos, F. Ferlaino, and R. N. Bisset, Alternating-domain supersolids in binary dipolar condensates, Phys. Rev. A **106**, 053322 (2022).

[36] P. Naidon and D. S. Petrov, Mixed Bubbles in Bose-Bose Mixtures, Phys. Rev. Lett. **126**, 115301 (2021).

[37] A. Ramanathan, K. C. Wright, S. R. Muniz, M. Zelan, W. T. Hill, C. J. Lobb, K. Helmerson, W. D. Phillips, and G. K. Campbell, Superflow in a Toroidal Bose-Einstein Condensate: An Atom Circuit with a Tunable Weak Link, Phys. Rev. Lett. **106**, 130401 (2011).

[38] K. C. Wright, R. B. Blakestad, C. J. Lobb, W. D. Phillips, and G. K. Campbell, Driving Phase Slips in a Superfluid Atom Circuit with a Rotating Weak Link, Phys. Rev. Lett. **110**, 025302 (2013).

[39] C. Ryu, P. W. Blackburn, A. A. Blinova, and M. G. Boshier, Experimental Realization of Josephson Junctions for an Atom SQUID, Phys. Rev. Lett. **111**, 205301 (2013).

[40] S. Komineas, N. R. Cooper, and N. Papanicolaou, Single vortex states in a confined Bose-Einstein condensate, Phys. Rev. A **72**, 053624 (2005).

[41] C. D'Errico, M. Zaccanti, M. Fattori, G. Roati, M. Inguscio, G. Modugno, and A. Simoni, Feshbach resonances in ultracold ^{39}K, New J. Phys. **9**, 223 (2007).

[42] L. Tanzi, C. R. Cabrera, J. Sanz, P. Cheiney, M. Tomza, and L. Tarruell, Feshbach resonances in potassium Bose-Bose mixtures, Phys. Rev. A **98**, 062712 (2018).

[43] S. Burger, K. Bongs, S. Dettmer, W. Ertmer, K. Sengstock, A. Sanpera, G. V. Shlyapnikov, and M. Lewenstein, Dark Solitons in Bose-Einstein Condensates, Phys. Rev. Lett. **83**, 5198 (1999).

[44] Z. Bai and R.-C. Li, Minimization principles for the linear response eigenvalue problem II: Computation, SIAM J. Matrix Anal. Appl. **34**, 392 (2013).

[45] Z. Bai and R.-C. Li, Minimization principles and computation for the generalized linear response eigenvalue problem, BIT Numer. Math. **54**, 31 (2014).

[46] A. J. Leggett, On the superfluid fraction of an arbitrary many-body system at $T = 0$, J. Stat. Phys. **93**, 927 (1998).

[47] F. Bloch, Superfluidity in a ring, Phys. Rev. A **7**, 2187 (1973).

[48] M. N. Tengstrand and S. M. Reimann, Droplet-superfluid compounds in binary bosonic mixtures, Phys. Rev. A **105**, 033319 (2022).

[49] D. Aghamalyan, M. Cominotti, M. Rizzi, D. Rossini, F. Hekking, A. Minguzzi, L.-C. Kwek, and L. Amico, Coherent superposition of current flows in an atomtronic quantum interference device, New J. Phys. **17**, 045023 (2015).

[50] M. Cominotti, D. Rossini, M. Rizzi, F. Hekking, and A. Minguzzi, Optimal Persistent Currents for Interacting Bosons on a Ring with a Gauge Field, Phys. Rev. Lett. **113**, 025301 (2014).

[51] F. Bloch, Josephson effect in a superconducting ring, Phys. Rev. B **2**, 109 (1970).

[52] L. Amico, D. Anderson, M. Boshier, J.-P. Brantut, L.-C. Kwek, A. Minguzzi, and W. von Klitzing, *Colloquium*: Atomtronic circuits: From many-body physics to quantum technologies, Rev. Mod. Phys. **94**, 041001 (2022).